

A Facile and Template-Free Hydrothermal Synthesis of Mn_3O_4 Nanorods on Graphene Sheets for Supercapacitor Electrodes with Long Cycle Stability

Jeong Woo Lee,^{†,‡} Anthony S. Hall,[‡] Jong-Duk Kim,^{*,†} and Thomas E. Mallouk^{*,‡}

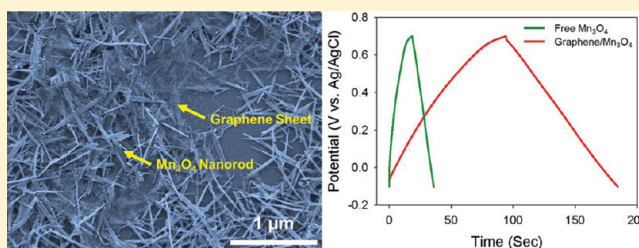
[†]Department of Chemical and Biomolecular Engineering, Center for Energy and Environment Engineering, Korea Advanced Institute of Science and Technology (KAIST), 291 Daehak-ro, Yuseong-gu, Daejeon 305-701, Republic of Korea

[‡]Department of Chemistry, The Pennsylvania State University, 104 Chemistry Building, University Park, Pennsylvania 16802, United States

S Supporting Information

ABSTRACT: Graphene/ Mn_3O_4 composites were prepared by a simple hydrothermal process from KMnO_4 using ethylene glycol as a reducing agent. Mn_3O_4 nanorods of 100 nm to 1 μm length were observed to be well-dispersed on graphene sheets. To assess the properties of these materials for use in supercapacitors, cyclic voltammetry and galvanostatic charging–discharging measurements were performed. Graphene/ Mn_3O_4 composites could be charged and discharged faster and had higher capacitance than free Mn_3O_4 nanorods. The capacitance of the composites was 100% retained after 10 000 cycles at a charging rate of 5 A/g.

KEYWORDS: Mn_3O_4 , graphene, nanorod, supercapacitor



1. INTRODUCTION

In the 21st century, energy storage has emerged as a key technological challenge. Because of the intrinsically high efficiency of electrochemical energy conversion and its compatibility with power generation from solar, wind, and nuclear resources, there is growing interest in the development of low-cost, high-power electrochemical energy-storage devices.¹ Among them, supercapacitors have received much attention for applications in hybrid electric vehicles, electrical vehicles, portable electronic devices, and backup power.²

There are two kinds of supercapacitors, which are differentiated by their charge-storage mechanisms. In electrical double-layer capacitors, charge is stored by rapid adsorption/desorption of electrolyte ions on high-surface-area carbon materials. In pseudocapacitors, charge is stored and released in Faradaic electron-transfer processes of a metal oxide or conducting polymer.³ It is also possible to combine carbon materials with metal oxides or conducting polymers. Supercapacitors deliver energy at high charge–discharge rates, so they have higher power density than other energy-storage devices such as lithium-ion batteries and fuel cells. However, they also have lower energy densities than batteries and fuel cells. Therefore, an important application of supercapacitors is to assist higher energy density storage devices under intermittent high-power conditions.

Among the pseudocapacitors, RuO_2 has been extensively studied in electrochemical capacitor electrodes because of its high specific capacitance.⁴ However, RuO_2 has the drawbacks of high cost and toxicity. Therefore, many studies have recently been directed toward replacing RuO_2 with inexpensive transition-metal

oxides such as nickel hydroxide,⁵ nickel oxide,⁶ cobalt hydroxide,⁷ cobalt oxide,⁸ and manganese oxide.⁹ For Faradaic redox reactions, nickel- and cobalt-related materials use alkaline electrolytes such as aqueous KOH, which have a potential window of 0.4–0.5 V. Because the energy density of a supercapacitor is proportional to the square of the cell voltage, the energy density of nickel- and cobalt-related materials is limited by the potential window.

Mn_3O_4 is a potentially interesting electrode material for electrolytic supercapacitors because of its low cost, environmental compatibility, and intrinsically high capacity.¹⁰ Table 1 summarizes some of the results that have been obtained to date with Mn_3O_4 as a supercapacitor electrode material. Except in thin films, the poor electronic conductivity limits the performance of Mn_3O_4 in terms of both capacitance and capacitance retention at high current density. A common strategy with poor electronic conductors such as transition-metal oxides is to combine them into composites with carbon, which is both lightweight and electronically conducting. The recent discovery of the interesting electronic, mechanical, and thermal properties of graphene sheets^{11–15} has stimulated research into its preparation as single sheets and composites and into the use of graphene as a conductive support for electrocatalysts and materials for electrochemical energy storage. Exfoliated graphene sheets combine exceptionally high surface area with electronic conductivity, are stable in electrochemical environments,

Received: December 10, 2011

Revised: February 11, 2012

Published: February 21, 2012

Table 1. Summary of Electrochemical Measurements Reported in Recent Papers for Mn₃O₄ Supercapacitor Electrodes

preparation method	nature of Mn ₃ O ₄	current collector	mass of electroactive materials (mg/cm ²)	electrolyte	measurement protocol ^a	maximum capacitance (F/g) ^b	capacitance retention after cycle test	ref (year)
electrostatic spray deposition	film	platinum-coated silicon water	0.116	0.1 M Na ₂ SO ₄	CV ($\nu = 50$ mV/s)	150	91% after 600 cycles	29 (2006)
hydrothermal	MWCNT/Mn ₃ O ₄ ^c powder	glassy carbon disk	0.01	2 M KCl	CV ($\nu = 5$ mV/s)	420	82% after 400 cycles	30 (2008)
hydrothermal	powder	graphite	0.25	1 M Na ₂ SO ₄	CV ($\nu = 500$ mV/s)	170	100% after 1500 cycles	31 (2008)
chemical bath deposition	film	borosilicate glass slides	0.57	1 M Na ₂ SO ₄	CV ($\nu = 10$ mV/s)	193		32 (2009)
successive ionic layer adsorption and reaction	film	stainless steel	0.45	1 M Na ₂ SO ₄	CV ($\nu = 5$ mV/s)	314		33 (2010)
precipitation from MnO ₂ organosol	graphene/Mn ₃ O ₄ ^d powder	platinum foil	0.75	1 M Na ₂ SO ₄	CV ($\nu = 5$ mV/s)	175		34 (2010)
hydrothermal	powder	graphite paper		6 M KOH		256		
chemical bath deposition	film	stainless steel	0.42	1 M Na ₂ SO ₄	CV ($\nu = 5$ mV/s)	322	100% after 1500 cycles	35 (2010)
hydrothermal	powder	glass carbon disk	0.01	2 M KCl	CV ($\nu = 5$ mV/s)	148	almost 100% after 400 cycles	37 (2011)
dip-casting method	MWCNT/Mn ₃ O ₄ ^c film	conductive tape with sputtered gold	10.1	0.5 M Na ₂ SO ₄	CV ($\nu = 2$ mV/s)	143	81% after 1000 cycles	38 (2011)
hydrothermal	graphene/Mn ₃ O ₄ ^d powder	nickel foam	2.0	1 M Na ₂ SO ₄	CV ($\nu = 5$ mV/s)	114	100% after 10 000 cycles	this work
					Cp ($i = 0.5$ A/g)	121		

^aCV = cyclic voltammetry, Cp = chronopotentiometry, ν = scan rate, and i = current density. ^bMaximum specific capacitance reported. ^cMultiwalled carbon nanotube (MWCNT)/Mn₃O₄ composite.

^dGraphene/Mn₃O₄ composite

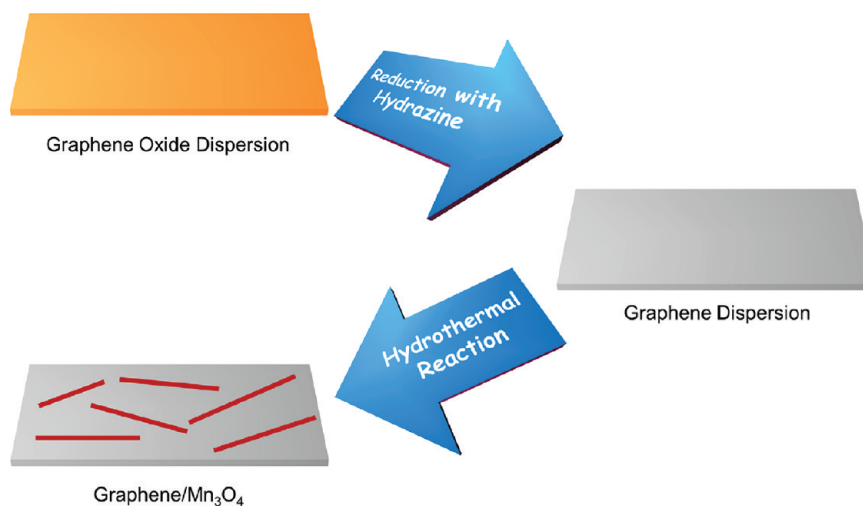


Figure 1. Schematic representation of the steps in the synthesis of GM composites.

and can be chemically functionalized. Composite materials of graphene and metal oxides are thus potentially important materials for high-energy-density as well as high-power electrochemical devices. Graphene-based composites including graphene/ $\text{Ni}(\text{OH})_2$,¹⁶ graphene/ SnO_2 ,¹⁷ and graphene/ MnO_2 ¹⁸ have been studied as electrode materials for supercapacitors. Gao and co-workers recently found that a graphene composite with nanoparticles of a Ni–Al layered double hydroxide (Ni–Al LDH) has good capacity retention when cycled at high current density.¹⁹ This property may be attributed to the growth of LDH nanosheets on the exfoliated graphene sheets, preventing restacking of the graphene sheets and facilitating electrolyte access to the electroactive $\text{Ni}^{2+/3+}$ ions in the LDH. In this study, we examine whether the same approach can be used to make supercapacitor electrode materials based on Mn_3O_4 , which can be used with acidic aqueous electrolytes. We report new graphene/ Mn_3O_4 composites and evaluate their charge–discharge properties and capacitance retention.

We prepared Mn_3O_4 nanorods on graphene sheets by a simple template-free hydrothermal reaction from KMnO_4 , using ethylene glycol as a reducing agent. The resulting Mn_3O_4 nanorods are well-dispersed on the graphene sheets, again preventing the sheets from restacking and providing electrolyte access to the electroactive oxide phase. When tested as supercapacitor electrode materials, these graphene/ Mn_3O_4 composite have 3–4 times higher capacitance than free Mn_3O_4 . Importantly, these materials also showed 100% capacitance retention after extensive cycling.

2. EXPERIMENTAL SECTION

2.1. Synthesis of Samples. Graphite oxide (GO) was obtained from natural graphite (Sigma-Aldrich) by a modification of the Hummers method.²⁰ The sequence of steps used to prepare the graphene/ Mn_3O_4 (GM) composite from GO is shown in Figure 1. A GO dispersion prepared by ultrasonication of 72 mg of GO in 80 mL of water was reduced to a dispersion of graphene sheets by adding aqueous ammonia (1 mL, 28–30 wt %) and hydrazine hydrate (1 mL) and heating in an oil bath at 95 °C for 2 h. After the reaction, the dispersion of graphene sheets was filtered. The collected solid was washed several times with water and then redispersed in 80 mL of water. A total of 0.002 mol of KMnO_4 was then dissolved in this dispersion. Ethylene glycol (2 mL) was added, and the suspension was stirred magnetically for 1 h at room temperature. The suspension was then transferred to a 125-mL-capacity Teflon-lined autoclave and

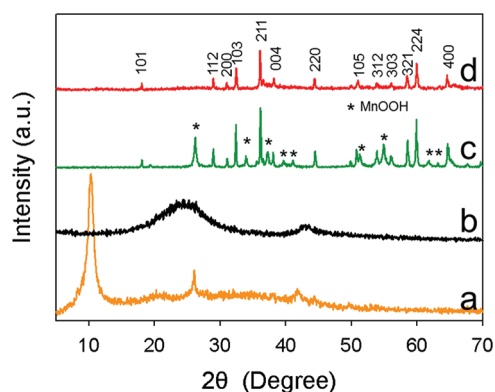


Figure 2. XRD patterns of (a) GO, (b) rGO, (c) free Mn_3O_4 , and (d) the GM composite.

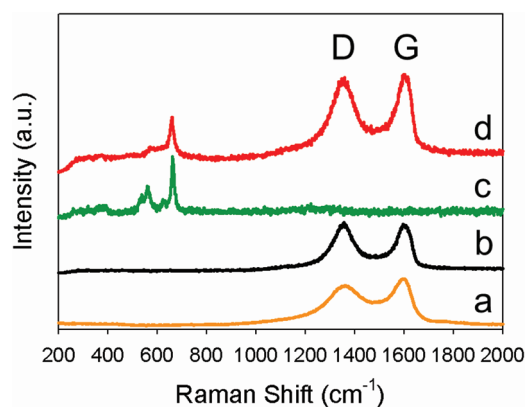


Figure 3. Raman spectra of (a) GO, (b) rGO, (c) free Mn_3O_4 , and (d) the GM composite.

heated under autogenous pressure to 120 °C for 4 h. After the reaction, the autoclave was allowed to cool to room temperature. The precipitate was washed with excess water and dried. Composites made with C/Mn molar ratios higher or lower than 3:1 gave lower specific capacitance. Free Mn_3O_4 and reduced graphene oxide (rGO) were prepared by the same method for comparison purposes.

2.2. Materials Characterization. X-ray diffraction (XRD) analysis was performed on a Philips X'Pert MPD powder X-ray diffractometer (Cu $K\alpha$, 40 kV, 40 mA). Raman spectra were obtained using a

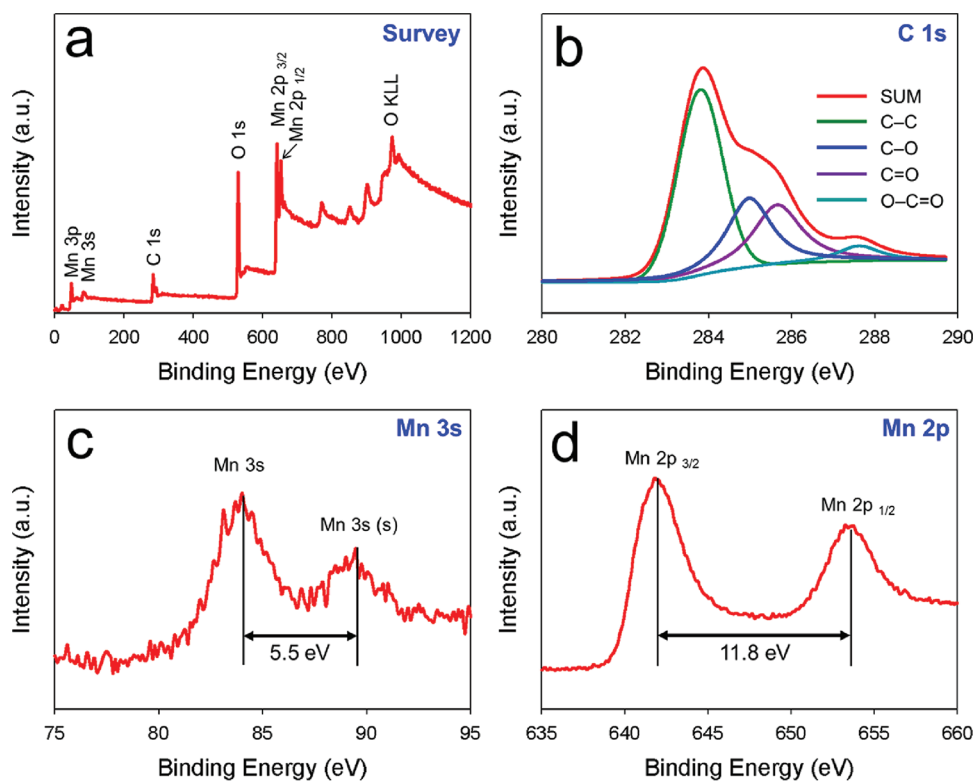


Figure 4. XPS spectra of the (a) survey scan, (b) C 1s region, (c) Mn 3s region, and (d) Mn 2p region of the GM composite.

LabRAM HR UV/vis/near-IR spectrometer (Horiba Jobin Yvon, France) with an argon-ion continuous-wave laser (514.5 nm) as the excitation source. X-ray photoelectron spectroscopy (XPS) was done with a Thermo VG Scientific Sigma Probe spectrometer. Transmission electron microscopy (TEM) images were taken on a JEOL 2010F microscope. Scanning electron microscopy (SEM) images were obtained on a Leo 1530 field-emission scanning electron microscope.

2.3. Preparation of Electrodes. To evaluate the electrochemical properties of the GM composites, working electrodes were fabricated as follows.¹⁹ The GM composite, carbon black, and poly(vinylidene fluoride) were mixed in a weight ratio of 85:10:5, using *N*-methyl-2-pyrrolidone as the solvent to yield a paste. This paste was incorporated in nickel foam (1 cm × 1 cm), and the mass of active material in the working electrode was 2.0 mg.

2.4. Evaluation of the Electrochemical Properties. Electrochemical characterization was done by cyclic voltammetry (CV) and by galvanostatic charging–discharging of half-cells using an EZStat potentiostat/galvanostat (Nuvant Systems, Inc.). A beaker-type three-electrode cell was equipped with a GM composite/nickel foam working electrode, an Ag/AgCl reference electrode (BASi), and platinum wire as the counter electrode. For all electrochemical measurements, 1 M Na₂SO₄ was used as the electrolyte and the experiments were done at ambient temperature, which was typically 23 °C. The specific capacitance was calculated by integrating the area under the CV curve to obtain the charge (*Q*) and then dividing by the mass of the electroactive material (*m*), the scan rate (*v*), and the potential window ($\Delta V = V_a - V_c$) according to eq 1.

$$C = \frac{Q}{\Delta V} = \frac{1}{mv(V_a - V_c)} \int_{V_a}^{V_c} I(V) dV \quad (1)$$

In addition, the specific capacitance can be calculated from the galvanostatic charging–discharging function according to eq 2.

$$C = \frac{I\Delta t}{\Delta Vm} \quad (2)$$

In this equation, *C* is the specific capacitance, *I* is the current, Δt is the discharging time, ΔV is the potential window, and *m* is mass of the electroactive material.

3. RESULTS AND DISCUSSION

Figure 2 shows XRD patterns of GO, rGO, free Mn₃O₄, and the GM composite. The GO pattern is dominated by a single broad peak at 10.3°, which corresponds to an interlayer distance of 0.86 nm (Figure 2a). The expansion of the galleries relative to the parent graphite (*d*₀₀₂ = 0.34 nm) is consistent with oxidation of the graphene sheets and intercalation of water. The pattern of the hydrazine-reduced rGO contains very broad reflections at 24° and 42° (corresponding to *d* spacings of 0.37 and 0.21 nm), indicating restacking to form a poorly ordered graphite-like material (Figure 2b). Figure 2c also shows the pattern of the solid material obtained by reacting KMnO₄ and ethylene glycol in the absence of graphene sheets. An initial product is observed when KMnO₄ and ethylene glycol are reacted at room temperature. After stirring for 1 h, amorphous and birnessite-type δ -MnO₂ were found (Figure S1a in the Supporting Information). When this material was washed with water (to remove excess ethylene glycol) and reacted hydrothermally, Mn₃O₄ was not obtained, and the sample remained a mixture of amorphous and δ -MnO₂ (Figure S1b in the Supporting Information). If the hydrothermal reaction was done without washing to remove ethylene glycol, Mn₃O₄ was obtained hydrothermally (120 °C, 4 h) by reduction of MnO₂ (Figure 2c). However, this Mn₃O₄ was not phase-pure, and the XRD pattern also showed the presence of MnOOH. On the other hand, when KMnO₄ and ethylene glycol were reacted under identical conditions in the graphene dispersion, the XRD pattern showed only the pure Mn₃O₄ phase (Figure 2d), which was found by electron microscopy (see below) to consist of nanorods that were well dispersed on the graphene sheets.

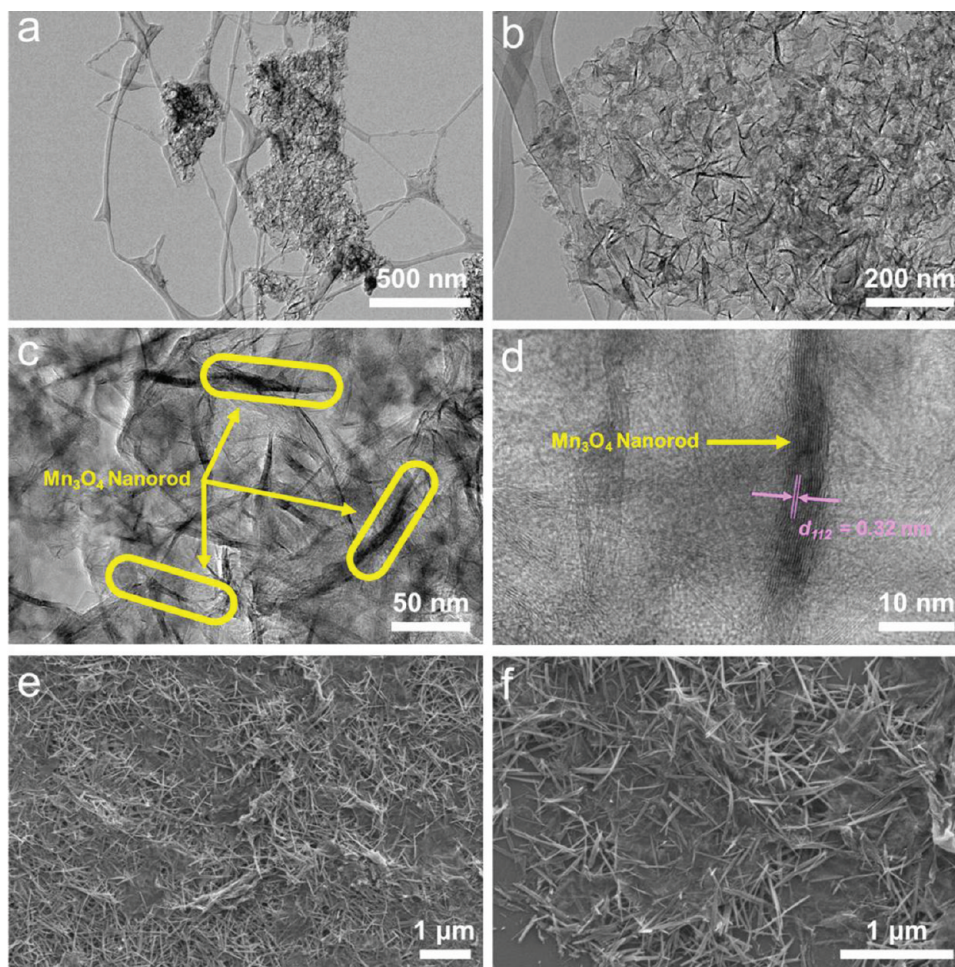


Figure 5. (a–d) TEM images and (e and f) SEM images of the GM composite.

Raman spectroscopy can be used to gain information about the structure of the graphene sheets in the GM composite and the precursor phases. Raman spectra of GO, rGO, free Mn_3O_4 , and the GM composite are shown in Figure 3. From the relative intensities of the D and G band peaks at 1350 and 1590 cm^{-1} , it can be concluded that the size of the sp^2 domains increases during reduction of GO.²¹ For free Mn_3O_4 , several peaks at 537.3 , 559.3 , and 621.4 cm^{-1} were observed and could be assigned to the presence of the MnOOH phase.²² Consistent with the XRD data, there are no peaks assignable to this phase in the GM composite. Strong peaks at 663.2 cm^{-1} were observed in both free Mn_3O_4 and the GM composite, which can be attributed to the Mn_3O_4 phase.²³

Figure 4 shows XPS spectra of the GM composite. In the survey region (0 – 1200 eV), carbon, manganese, and oxygen were detected. Deconvolution of the C 1s peak (Figure 4b) shows the presence of nonoxygenated carbon at 284.5 eV, carbon in C–O (hydroxyl and epoxy groups) at 285.7 eV, C=O (carbonyl groups) at 286.4 eV, and O–C=O (carboxyl groups) at 288.3 eV. The intensities of these peaks are smaller than those in GO (Figure S2b in the Supporting Information), consistent with reduction of GO. The manganese oxidation state was confirmed from the multiplet splitting of the Mn 3s peak. This splitting arises from exchange interaction between the remaining electron in the 3s orbital and the other unpaired electrons, which all have parallel spins.²⁴ The splitting width is 5.5 eV, which is in accordance with a previous report on the

XPS spectrum of Mn_3O_4 .²⁵ In the Mn 2p region, a $2\text{p}_{3/2}$ – $2\text{p}_{1/2}$ doublet at 653.7 and 642.9 eV is observed, and the splitting width (11.8 eV) is in agreement with an earlier report on Mn_3O_4 .²⁵

Parts a–d of Figure 5 show TEM images of GM composites at different magnifications. These images show well-dispersed nanorods on the graphene sheets. An enlarged TEM image shows lattice fringes with a d spacing of 0.32 nm, corresponding to the (112) planes of Mn_3O_4 crystals. In the SEM images, long thin nanorods can be clearly seen, which are similar to those in the TEM images. From the TEM and SEM images, the diameters of the individual nanorods are in the range of 5 – 30 nm, their lengths are 100 nm to 1 μm , and their aspect ratios are in most cases greater than 10 . Most of the samples consist of nanorods, but there are also some octahedral crystals with edge lengths of 100 – 200 nm (Figure S3 in the Supporting Information). The synthesis of Mn_3O_4 nanorods has been previously reported using surfactants^{26,27} and also in a two-step hydrothermal process similar to that reported here.²⁸ In the latter study, the initial reaction of KMnO_4 and poly(ethylene glycol) at ambient temperature gave a mixture of Mn_3O_4 and MnOOH , and subsequent hydrothermal treatment gave phase-pure Mn_3O_4 nanorods.²⁸ We observed a similar sequence of product phases using ethylene glycol as the reducing agent.

CV and galvanostatic charging–discharging measurements were performed to compare free Mn_3O_4 and the GM composite at 50 mV/s scan rate in 1 M Na_2SO_4 , and the results are

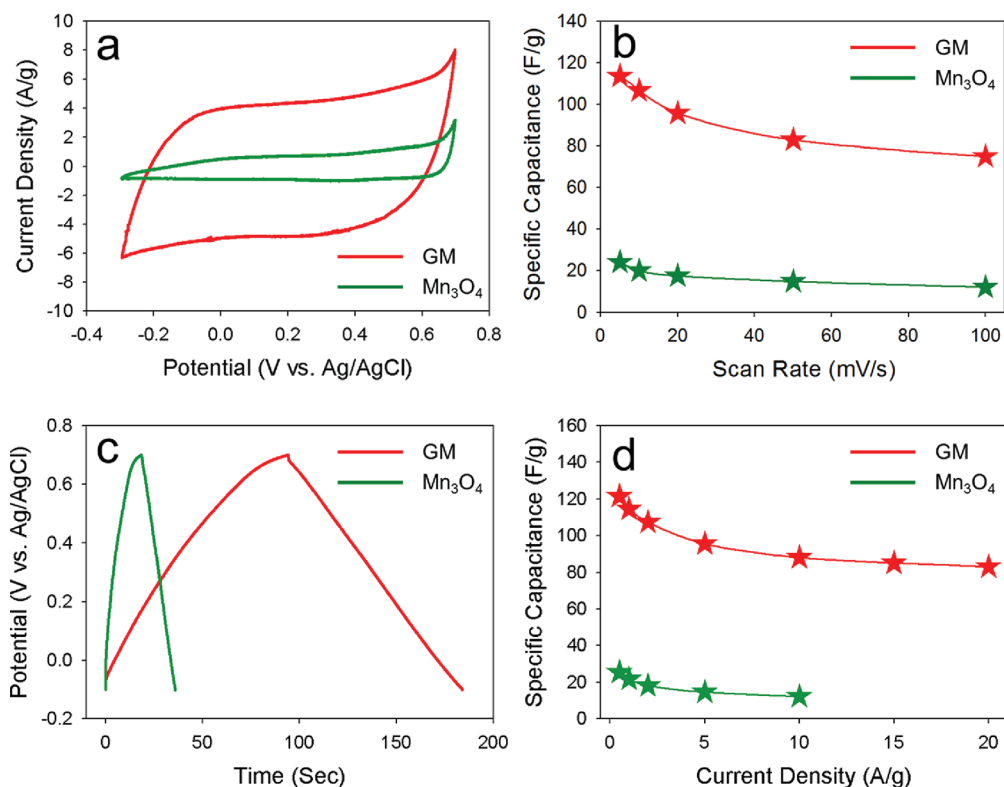


Figure 6. Supercapacitive properties of free Mn₃O₄ and the GM composite: (a) CV curves at 50 mV/s scan rate; (b) specific capacitance variation at different scan rates; (c) galvanostatic charging–discharging curves at 1 A/g current density; (d) specific capacitance variation at different current densities.

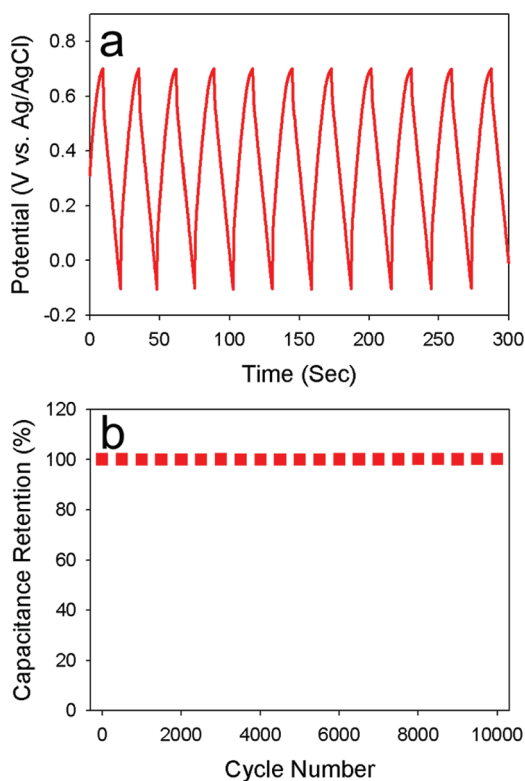


Figure 7. Cycle test of the GM composite: (a) galvanostatic charging–discharging curve at a nominal charging rate of 5 A/g; (b) variation in the capacitance retention as function of the cycle number.

shown in Figure 6. The specific capacitance is proportional to the area under the CV curve, which is clearly much larger for

the GM composite than for free Mn₃O₄ (Figure 6a) or rGO (Figure S4 in the Supporting Information). Figure 6b shows the specific capacitance of free Mn₃O₄ and the GM composite as a function of the scan rate. The latter had 3–4 times higher specific capacitance at scan rates between 5 and 100 mV/s. Galvanostatic charging–discharging is a complementary method for measuring the specific capacitance of electrochemical capacitors at constant current. Figure 6c shows galvanostatic charging–discharging curves of free Mn₃O₄ and the GM composite at 1 A/g current density. The increase in the charging time represents the higher capacitance of the GM composite. The specific capacitance is shown as a function of the current density in Figure 6d. The specific capacitance of free Mn₃O₄ was 25, 22, 18, 15, and 12 F/g at 0.5, 1, 2, 5, and 10 A/g current density, respectively. For current densities beyond 10 A/g, the *iR* drop was too large to permit an accurate calculation of the specific capacitance. In contrast, the specific capacitance of the GM composite was 121, 115, 107, 97, 88, 85, and 83 F/g at 0.5, 1, 2, 5, 10, 15, and 20 A/g, respectively. The increase in the specific capacitance at high current density can be attributed to the conductivity of the graphene sheets.

Importantly, the specific capacitance was measured at a high mass loading of 2.0 mg/cm², which is higher than that investigated in other recent reports on Mn₃O₄.^{29–37} High loading implies a thick electrode film, which exacerbates the problems of electrode and electrolyte contact to the bulk electroactive material. In addition, a high specific capacitance is observed at current densities beyond 10 A/g, where there are no prior reports on Mn₃O₄ using galvanostatic measurement. These data are important for assessing the viability of Mn₃O₄ in bulk supercapacitor electrodes.

Because a long cycle life is among the most important criteria for a supercapacitor, an endurance test was conducted using

galvanostatic charging–discharging cycles at 5 A/g (Figure 7a). During the first 1000 cycles, the specific capacitance increased slightly and was maintained at the same value over the next 9000 cycles. Thus, over 10 000 cycles, the capacitance retention was slightly over 100% (Figure 7b). This contrasts with experiments on other kinds of Mn_3O_4 electrodes, where there is significant degradation of the capacitance in 400–1000 cycle tests.^{29,30,38} We postulate two effects of the graphene component in promoting a high capacity and a long cycle life for Mn_3O_4 composites. First, the graphene sheets serve as a conductive matrix to promote fast Faradaic charging and discharging of the Mn_3O_4 nanorods. Second, the graphene inhibits aggregation of the Mn_3O_4 nanorods, preserving the high-surface-area interface between the Mn_3O_4 nanorods and the electrolyte.

4. CONCLUSIONS

We prepared Mn_3O_4 nanorods on graphene sheets by a simple template-free hydrothermal reaction from KMnO_4 , using ethylene glycol as the reducing agent. The Mn_3O_4 nanorods were 5–30 nm in diameter, and their lengths were 100 nm to 1 μm . CV and galvanostatic charging–discharging measurements were performed to characterize these materials as supercapacitor electrodes. Relative to free Mn_3O_4 , the GM composite showed 4 times higher capacitance, had substantially higher power density, and had outstanding capacitance retention upon cycling.

■ ASSOCIATED CONTENT

Supporting Information

XRD patterns, XPS spectra, an SEM image, and CV curves. This material is available free of charge via the Internet at <http://pubs.acs.org>.

■ AUTHOR INFORMATION

Corresponding Author

*E-mail: jdkim@kaist.ac.kr (J.-D.K.), tem5@psu.edu (T.E.M.).

Notes

The authors declare no competing financial interest.

■ ACKNOWLEDGMENTS

This work was supported by the National Science Foundation under Grant CHE-0910513 and by the BK 21 program and Basic Science Research Program through the National Research Foundation of Korea funded by the Ministry of Education, Science and Technology (Grant 2009-0076882).

■ REFERENCES

- (1) Dunn, B.; Kamath, H.; Tarascon, J.-M. *Science* **2011**, *334*, 928.
- (2) Liu, R.; Duay, J.; Lee, S. B. *Chem. Commun.* **2011**, *47*, 1384.
- (3) (a) Zhao, X.; Sanchez, B. M.; Dobson, P. J.; Grant, P. S. *Nanoscale* **2011**, *3*, 839. (b) Wang, G.; Zhang, L.; Zhang, J. *Chem. Soc. Rev.* **2012**, *41*, 797.
- (4) Wu, Z.-S.; Wang, D.-W.; Ren, W.; Zhao, J.; Zhou, G.; Li, F.; Cheng, H.-M. *Adv. Funct. Mater.* **2010**, *10*, 3595.
- (5) (a) Lee, J. W.; Ko, J. M.; Kim, J.-D. *J. Phys. Chem. C* **2011**, *115*, 19445. (b) Wang, H.; Casalongue, H. S.; Liang, Y.; Dai, H. *J. Am. Chem. Soc.* **2010**, *132*, 7472.
- (6) (a) Lee, J. W.; Ahn, T.; Kim, J. H.; Ko, J. M.; Kim, J.-D. *Electrochim. Acta* **2011**, *56*, 4849. (b) Kim, J.-H.; Zhu, K.; Yan, Y.; Perkins, C. L.; Frank, A. J. *Nano Lett.* **2010**, *10*, 4099.
- (7) (a) Hu, Z.-A.; Xie, Y.-L.; Wang, Y.-X.; Xie, L.-J.; Fu, G.-R.; Jin, X.-Q.; Zhang, Z.-Y.; Yang, Y.-Y.; Wu, H.-Y. *J. Phys. Chem. C* **2009**, *113*, 12502. (b) Chen, S.; Zhu, J.; Wang, W. *J. Phys. Chem. C* **2010**, *114*, 11829.
- (8) (a) Meher, S. K.; Rao, G. R. *J. Phys. Chem. C* **2011**, *115*, 15646. (b) Wei, T.-Y.; Chen, C.-H.; Chang, K.-H.; Lu, S.-Y.; Hu, C.-C. *Chem. Mater.* **2009**, *21*, 3228.
- (9) (a) Chen, S.; Zhu, J.; Han, Q.; Zheng, X.; Yang, Y.; Wang, X. *Cryst. Growth Des.* **2009**, *9*, 4356. (b) Zhang, J.; Jiang, J.; Zhao, X. S. *J. Phys. Chem. C* **2011**, *115*, 6448.
- (10) Brock, S. L.; Duan, N.; Tian, Z. R.; Giraldo, O.; Zhou, H.; Suib, S. L. *Chem. Mater.* **1998**, *10*, 2619.
- (11) Jung, I.; Dikin, D. A.; Piner, R. D.; Ruoff, R. S. *Nano Lett.* **2008**, *8*, 4283.
- (12) Novoselov, K. S.; Jiang, Z.; Zhang, Y. S.; Morozov, V.; Stormer, H. L.; Zeitler, U.; Maan, J. C.; Boebinger, G. S.; Kim, P.; Geim, A. K. *Science* **2007**, *315*, 1379.
- (13) Lee, C.; Wei, X.; Kysar, J. W.; Hone, J. *Science* **2008**, *321*, 385.
- (14) Stoller, M. D.; Park, S.; Zhu, Y.; An, J.; Ruoff, R. S. *Nano Lett.* **2008**, *8*, 3498.
- (15) Balandin, A. A.; Ghosh, S.; Bao, W. Z.; Calizo, I.; Teweldebrhan, D.; Miao, F.; Lau, C. N. *Nano Lett.* **2008**, *8*, 902.
- (16) Lee, J. W.; Ahn, T.; Soundararajan, D.; Ko, J. M.; Kim, J.-D. *Chem. Commun.* **2011**, *47*, 6305.
- (17) Wang, S.; Jiang, S. P.; Wang, X. *Electrochim. Acta* **2011**, *56*, 3338.
- (18) Zhang, J.; Jiang, J.; Zhao, X. S. *J. Phys. Chem. C* **2011**, *115*, 6448.
- (19) Gao, Z.; Wang, J.; Li, Z.; Yang, W.; Wang, B.; Hou, M.; He, Y.; Mann, T.; Yang, P.; Zhang, M.; Liu, L. *Chem. Mater.* **2011**, *23*, 3509.
- (20) Hummers, W. S.; Offeman, R. E. *J. Am. Chem. Soc.* **1958**, *80*, 1339.
- (21) Gao, J.; Liu, F.; Liu, Y.; Ma, N.; Wang, Z.; Zhang, X. *Chem. Mater.* **2010**, *22*, 2213.
- (22) Gao, T.; Krumeich, F.; Nesper, R.; Fjellvag, H.; Norby, P. *Inorg. Chem.* **2009**, *48*, 6242.
- (23) Nam, K.-W.; Kim, M. G.; Kim, W.-B. *J. Phys. Chem. C* **2007**, *111*, 749.
- (24) Toupin, M.; Brousse, T.; Belanger, D. *Chem. Mater.* **2002**, *14*, 3946.
- (25) Raj, A. M. E.; Victoria, S. G.; Jothy, V. B.; Ravidhas, C.; Wollschlager, J.; Suendorf, M.; Neumann, M.; Jayachandran, M.; Sanjeeviraja, C. *Appl. Surf. Sci.* **2010**, *256*, 2920.
- (26) Dong, X.; Zhang, X.; Liu, B.; Wang, H.; Li, Y.; Huang, Y.; Du, Z. *J. Nanosci. Nanotechnol.* **2006**, *6*, 818.
- (27) Chen, Z. W.; Lai, J. K. L.; Shek, C. H. *Appl. Phys. Lett.* **2005**, *86*, 181911.
- (28) Du, J.; Gao, Y.; Chai, L.; Zou, G.; Li, Y.; Qian, Y. *Nanotechnol.* **2006**, *17*, 4923.
- (29) Nam, K.-W.; Kim, K.-B. *J. Electrochem. Soc.* **2006**, *153*, A81.
- (30) An, G.; Yu, P.; Xiao, M.; Liu, Z.; Miao, Z.; Ding, K.; Mao, L. *Nanotechnology* **2008**, *19*, 275709.
- (31) Hu, C.-C.; Wu, Y.-T.; Chang, K.-H. *Chem. Mater.* **2008**, *20*, 2890.
- (32) Dubal, D. P.; Dhawale, D. S.; Salunkhe, R. R.; Pawar, S. M.; Fulari, V. J.; Lokhande, C. D. *J. Alloys Compd.* **2009**, *484*, 218.
- (33) Dubal, D. P.; Dhawale, D. S.; Salunkhe, R. R.; Pawar, S. M.; Lokhande, C. D. *Appl. Surf. Sci.* **2010**, *256*, 4411.
- (34) Wang, B.; Park, J.; Wang, C.; Ahn, H.; Wang, G. *Electrochim. Acta* **2010**, *55*, 6812.
- (35) Jiang, H.; Zhao, T.; Yan, C.; Ma, J.; Li, C. *CrystEngComm* **2010**, *2*, 2195.
- (36) Dubal, D. P.; Dhawale, D. S.; Salunkhe, R. R.; Fulari, V. J.; Lokhande, C. D. *J. Alloys Compd.* **2010**, *497*, 166.
- (37) Fang, M.; Tan, X.; Liu, M.; Kang, S.; Hu, X.; Zhang, L. *CrystEngComm* **2011**, *13*, 4915.
- (38) Cui, X.; Hu, F.; Wer, W.; Chen, W. *Carbon* **2011**, *49*, 1225.